minerals

MDPI

Article

Coal Facies and Coal-Forming Environment Evolution of Deep Coals in Shanxi Formation Member 2, Daning–Jixian Block, Southeastern Ordos Basin

Wei Hou [1,2], Mansheng Wu [1,2], Lei Zhang [1,2], Yuan Wang [1,2], Shan Jiang [3], Shirui Liu [1,2], Zengping Zhao [1,2], Jie Yin [3,*] and Xiaosong Shi [1,2]

[1] China United Coalbed Methane National Engineering Research Center Co., Ltd., Beijing 100095, China
[2] PetroChina Coalbed Methane Company Limited, Beijing 100028, China
[3] School of Geosciences, Yangtze University, Wuhan 430100, China
* Correspondence: yinjiecr7@yangtzeu.edu.cn

Abstract

The Daning–Jixian Block in the southeastern Ordos Basin hosts abundant deep CBM resources. Characterizing coal facies types and peat-forming environments provides critical evidence for analyzing deep coalbed methane genesis and optimizing prospective favorable areas. This study focuses on the No. 5 coal seam within the Shan 2 Member (S2) of the Permian Shanxi Formation in the Daning–Jixian Block and conducts a high-resolution spatiotemporal analysis of the relationships among depositional environments, peat-forming environments, and coal facies. Multiple technical approaches, including INPEFA filtering based on maximum entropy spectral analysis, wavelet transform (WT) for the analysis of high-frequency well-log cycles, quantitative identification of coal macerals, and coal quality geochemical analyses, are comprehensively adopted to establish a high-resolution sequence stratigraphic framework. Combined with two coal facies discrimination diagrams (GI-TPI and GWI-VI), the interdistributary bay paleoenvironment for coal accumulation is reconstructed in detail. The research results show that: (1) The Shan 2 Member (S2) develops a typical meandering river delta front–shallow lagoon sedimentary system constrained by paleogeomorphology, which can be divided into four fourth-order sequences ($S2^4$,$S2^3$,$S2^2$,$S2^1$), recording the full evolutionary sequence of the distributary-channel system: progradational erosion, channel abandonment and bay formation, bay shallowing and mire development, and secondary progradation.(2) The No. 5 coal seam is characterized by ultra-low sulfur and medium-low ash content, and the coal facies parameters follow a distribution pattern of high Gelification Index (GI), extremely low Groundwater Influence Index (GWI), and widely varying Tissue Preservation Index (TPI). (3) The coal facies are dominated by an assemblage of wet forest mires and herbaceous mires, indicating that peat-forming mires likely developed under weakly reducing, stagnant, freshwater-dominated conditions sheltered by paleogeomorphic highs. This study indicates that the large-scale lateral abandonment of subaqueous distributary channels on the meandering delta front and the shallowing of lagoon–interdistributary-bay depressions constitute the key dynamic mechanisms controlling the regional, continuous development of high-quality, thick coal seams characterized by high GI and low GWI. This understanding of the depositional processes and environments provides a theoretical basis for optimizing and geologically evaluating favorable reservoir zones for deep coalbed methane.

Keywords: Daning–Jixian Block; Shan 2 Member; meandering river delta; coal facies types; coal accumulation model

Check for updates

Academic Editor: Thomas Gentzis

Received: 19 August 2026
Revised: 23 September 2026
Accepted: 1 October 2026
Published: 6 October 2026

Copyright: © 2026 by the authors. Licensee MDPI, Basel, Switzerland. This article is an open access article distributed under the terms and conditions of the Creative Commons Attribution (CC BY) license.

1. Introduction

Deep coalbed methane (CBM) refers to a self-generated and self-stored unconventional natural gas hosted within coal seams. Major exploration breakthroughs for deep CBM have been achieved in the Ordos Basin in recent years, revealing promising resource prospects. The depositional environments of coal-bearing strata and the coal facies developed within them are key controls on coalbed methane enrichment. By controlling key conditions in peat-forming mires, including hydrodynamic and redox conditions, these depositional environments directly influence the macroscopic characteristics and maceral composition of coal seams, thereby affecting their gas-bearing capacity and pore-structure characteristics. Carrying out high-precision reconstruction of depositional environments and characterization of coal facies constitutes a vital geological foundation for systematically revealing the enrichment regularity of deep coalbed methane and optimizing favorable reservoir zones within coal seams [1–3].

At present, existing sedimentological investigations on coal-bearing strata along the eastern margin of the Ordos Basin are mostly restricted to macroscale descriptions of subfacies, including delta front, delta plain, and lagoon-tidal flat [4–6]. These studies provide limited predictive guidance for the detailed subdivision of small-scale peat-forming microenvironments and the lateral distribution of coal facies within coal seams. In addition, the reconstruction of paleopeat depositional environments relying on a single coal facies parameter or conventional macroscopic facies identification suffers from multiple solutions and inherent limitations. Because marine–continental transitional coal-bearing strata commonly contain multiple transgressive–regressive cycles, frequent sandstone–mudstone interbedding, and complex sedimentary rhythms, conventional manual sequence division is often subjective and has limited resolution. Treating well-log signals as high-frequency time series, together with progressive multi-index analysis integrating maceral quantification, microscopic observations, proximate analysis, and sulfur geochemistry, provides an effective approach for reconstructing the evolution of peat-forming environments.

This study focuses on the coal-bearing succession of the Lower Permian Shanxi Formation, particularly the No. 5 coal seam, in the Daning–Jixian Block, eastern Ordos Basin. A high-resolution sequence stratigraphic framework was established using inflection points and extrema of the Integrated Prediction Error Filter Analysis (INPEFA) residual curves derived from Maximum Entropy Spectral Analysis (MESA), together with time–frequency analysis of wavelet-transform (WT) signals. This framework was then used to trace the lateral distribution and evolution of sedimentary microfacies within the Shan 2 Member (S2) [7–12]. Scanning electron microscopy (SEM), quantitative elemental analysis, ash-yield determination, and total- and morphological-sulfur analyses were subsequently conducted to obtain information on the evolution of water depth, hydrodynamic intensity, and redox conditions. The Tissue Preservation Index (TPI) and Gelification Index (GI) were used to construct coal-facies diagrams and identify specific coal-facies types. Finally, the sequence stratigraphic framework, sedimentary-facies evolution, and coal-facies distribution were integrated to establish a spatial and temporal evolutionary model linking sequence framework, depositional environment, peat-forming mire type, and coal facies. This model clarifies the controls exerted by paleoclimate, relative sea-level fluctuations, and tectonic subsidence on peat accumulation and coal-facies development and provides a basis for evaluating favorable deep coalbed methane reservoir zones.

2. Geological Setting

The Ordos Basin is located in the western North China Craton (Figure 1a). It is bounded by the Lüliang Mountains to the east, extends westwards to the Tengger Desert, reaches the Yin Mountains to the north, and extends southward to the Qinling Mountains

(Figure 1b) [13]. The basin extends mainly in a north–south direction and is characterized by stable tectonic conditions and a well-developed sedimentary cover, making it a typical cratonic inland sedimentary basin [14,15]. The tectonic framework of the Ordos Basin consists of several first-order structural units, including the Tianhuan Depression, the western thrust belt, the Yishan Slope, and the Western Shanxi Fold Depression Belt. The Daning–Jixian Block is situated in the southern section of the Western Shanxi Fold Belt on the eastern margin of the basin, adjoining the southeastern margin of the Yi-Shan Slope. The block exhibits an overall gentle tectonic morphology dominated by a monocline structure. The stratigraphic dip ranges from 1° to 2° in the western area and gradually increases eastward to 10–15°. The regional tectonic framework exhibits the characteristics of "one uplift, one depression and two slopes" which is governed by secondary tectonic units including the Taoyuan Anticline Belt, the Puxian Sag, the Eastern Slope Belt, and the Western Gentle Slope Belt (Figure 1c). The No. 5 coal seam is an important target interval for deep coalbed methane in the Shanxi Formation and formed within the delta-front depositional system of the S2. The widely distributed No. 5 coal seam occurs at burial depths of 1700–2400 m and ranges from 1.0 to 6.0 m in thickness. Its thickness varies irregularly across the block, mainly owing to the migration of interdistributary-bay peat-forming mires, making it a favorable target for deep coalbed methane exploration within the Shanxi Formation (Figure 1d) [16,17].

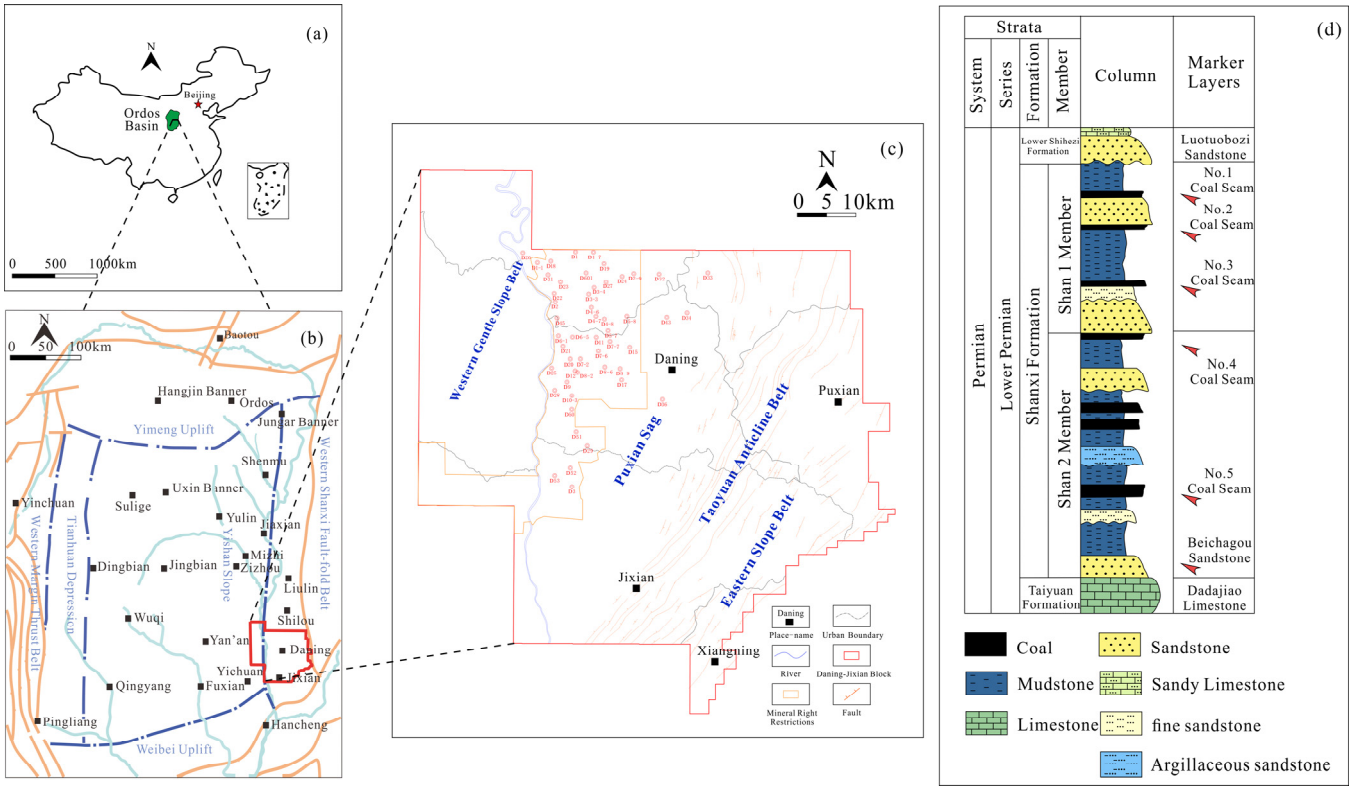


Figure 1. Location, tectonic framework, and stratigraphy of the Daning–Jixian Block. (**a**) Location of the Ordos Basin in China; (**b**) first-order tectonic units of the Ordos Basin; (**c**) structural framework and well locations in the Daning–Jixian Block; (**d**) comprehensive stratigraphic column of the Shanxi Formation.

3. Samples and Experimental Methods

3.1. Samples

A detailed geological characterization was carried out based on data from 46 key single wells in the Daning–Jixian Block. A total of 28 coal samples were collected from the No. 5 Coal seam, covering wells D3-4, D5-1, D54, D57, D61, D62, D63, D64 and D7-11 (Figure 1a).

3.2. Experiments and Methods

This study integrates multiple analytical approaches including time–frequency multi-information fusion of well-log signals, macroscopic and microscopic core observations, and coal geochemical tests for comprehensive analysis. With regard to the establishment of a high-resolution sequence stratigraphic framework and identification of sedimentary microfacies, this study mainly adopts the Integrated Prediction Error Filter Analysis (INPEFA) of GR logs based on Maximum Entropy Spectral Analysis (MESA), alongside Wavelet Transform (WT) time–frequency analysis techniques, and combines these with physical core observations of core samples to classify sedimentary microfacies. With regard to the identification of peat-forming microenvironments and coal facies types, multiple tests were synchronously carried out, including quantitative maceral identification on polished coal pellets, high-resolution field emission scanning electron microscopy (FE-SEM; FEI Quanta FEG 450, Hillsboro, OR, USA) observation, proximate analysis of coal, and quantitative determination of sulfur contents. Key coal facies indices were further calculated based on the above test data to complete crossplot projection analysis.

3.2.1. Integrated Prediction Error Filter Analysis (INPEFA)

The S2 in the Daning–Jixian Block represents typical marine–continental transitional coal-bearing deposits with frequent multistage transgression-regression cycles. This interval is characterized by frequent interbedded sandstone and mudstone and complex sedimentary rhythms. As a result, conventional manual sequence classification has limited resolution and strong subjectivity. Therefore, one-dimensional well-log signals such as GR logs are regarded as depth sequences carrying high-frequency sedimentary geological information in this study [9,11]. Relying on the high-resolution spectral decomposition advantages of Maximum Entropy Spectral Analysis provides a detailed characterization of the evolution of stratigraphic cycles. The specific calculation workflow consists of three steps. First, MESA is applied to smooth and predict the raw GR logging curves to weaken random noise interference and improve the accuracy of cycle identification. Second, difference operation is performed between the measured logging response values and MESA smoothed predicted values to extract highly sensitive high-frequency residual sequences. Finally, the residual sequences are integrated along the depth direction to generate INPEFA curves, which can effectively highlight subtle sedimentary cycles and long-term base-level evolution trends that are difficult to identify from raw logging curves [7,9,10].

Trends and extrema in the INPEFA curves allow sequence boundaries and key depositional surfaces at different hierarchical levels within the S2 marine–continental transitional succession to be identified quantitatively and systematically. The specific identification criteria are as follows: (1) a sustained positive trend, characterized by progressively increasing GR values and mud content, indicates transgression; (2) a negative inflection point at which the GR response reaches a maximum and marks a maximum flooding surface; (3) a sustained negative trend, characterized by progressively decreasing GR values and increasing sand content, indicates regression and progradation; and (4) a positive inflection point at which the GR response reaches a minimum and marks a fourth-order or higher-frequency sequence boundary and the onset of a new depositional cycle [7,9,10]. The S2 succession contains frequent interbeds of sandstone, mudstone, and coal. Because

GR logs are highly sensitive to changes in mud content and lithological cyclicity, GR data were selected as the primary dataset for high-frequency sequence subdivision and detailed interwell correlation.

3.2.2. Wavelet Transform

WT is introduced to convert one-dimensional GR curves into a two-dimensional time–frequency domain, which can extract the evolution law of signal spectra with depth and further reveal multi-scale stratigraphic cyclic architectures [10,12]. The mathematical integral formula of Continuous Wavelet Transform is expressed as follows:

$$WT_f(a,b) = \frac{1}{|a|^{1/2}} \int_{-\infty}^{+\infty} f(t)\psi\left(\frac{t-b}{a}\right) dt (a \neq 0) \quad (1)$$

where $f(t)$ represents the signal to be analyzed, $\psi(t)$ denotes the mother wavelet function, a is the scale factor (controlling the compression or stretching of signals), and b refers to the translation factor (controlling the temporal position of signals). A large scale factor a stretches the wavelet function and corresponds to low-frequency, long-period components; in contrast, a small value of a compresses the wavelet function and matches high-frequency, short-period components.

3.2.3. Quantitative Maceral Determination and Microscopic Characterization

With regard to the identification of organic components, bulk coal samples were prepared into polished coal pellets. According to the standard ISO 7404-3:2009 [18], fine quantitative identification and volume percentage measurement of macerals and sub-macerals were performed under oil immersion reflected light using a polarizing microscope. The classification of macerals was carried out in accordance with the International Committee on Coal Petrology (ICCP System 1994) guidelines [19,20]. The relative contents of vitrinite (including telinite, collinite, desmocollinite and other sub-macerals) and inertinite (including fusinite, semifusinite, inertodetrinite, macrinite and other sub-macerals) were counted (Table 1). Field-emission scanning electron microscopy (FE-SEM; FEI Quanta FEG 450, Hillsboro, OR, USA) was employed to characterize pore morphology, mineral occurrence, and the textural relationships between mineral phases and the coal matrix in fresh coal samples [21]. On the basis of these observations, pyrite genesis was evaluated according to crystal morphology, mode of occurrence, and association with clastic or alteration minerals. Framboidal or finely disseminated pyrite enclosed within the coal matrix was interpreted as syngenetic to early diagenetic; rounded or abraded grains associated with clastic minerals were considered detrital; and coarse crystalline, vein- or fracture-filling pyrite associated with alteration minerals was interpreted as late diagenetic to hydrothermal [22].

Table 1. Maceral contents and V/I Ratio of No. 5 coal seam.

Sample	V	I	L	M	V/I
D3-4-1	78.15	20.31	0.00	1.54	3.85
D3-4-2	54.95	5.61	1.87	37.57	9.80
D5-1-1	90.43	7.47	0.57	1.53	12.11
D5-1-2	82.32	16.54	0.19	0.95	4.98
D5-1-3	92.07	5.53	0.00	2.40	16.65
D5-1-4	83.28	7.41	1.71	7.60	11.24
D7-11-1	90.34	6.25	0.00	3.41	14.45
D57-1	83.66	11.84	0.00	4.50	7.06
D57-2	94.67	2.53	0.00	2.80	37.46
D57-3	92.37	6.43	0.00	1.20	14.37

Table 1. *Cont.*

Sample	V	I	L	M	V/I
D57-4	89.86	6.14	0.00	4.00	14.64
D61-1	66.40	22.40	1.60	9.60	2.96
D61-2	87.60	7.00	1.60	3.80	12.51
D61-3	72.00	14.80	2.00	11.20	4.86
D62-1	78.80	14.90	0.00	6.30	5.29
D62-2	90.80	6.30	0.00	2.90	14.41
D63-1	86.52	12.06	0.00	1.42	7.17
D64-1	62.16	31.27	0.00	6.57	1.99
D64-2	73.40	19.22	0.00	7.38	3.82
D64-3	85.36	10.65	0.00	3.99	8.02
D64-4	65.34	26.29	0.00	8.37	2.49
D64-5	73.03	8.27	0.00	18.70	8.83

3.2.4. Proximate Analysis, Sulfur Determination and Coal Facies Calculation

In accordance with the national standard GB/T 30732-2014 [23], proximate analysis of coal and quantitative sulfur measurement of coal samples are carried out to accurately determine air-dried basis moisture (M_{ad}), dry basis ash yield (A_d), dry ash-free basis volatile matter (V_{daf}), dry basis fixed carbon (FC_d) and total sulfur content on dry basis ($S_{t,d}$) of the coal samples [24]. Total sulfur contents were interpreted in conjunction with pyrite morphology and occurrence, mineral assemblages, sedimentary microfacies, maceral composition, and the regional structural framework to constrain the paleowater salinity and redox conditions during peat accumulation. The measured total sulfur data were classified into six grades by referring to coal sulfur classification criteria (Table 2): ultra-low sulfur coal (≤0.50%), low sulfur coal (0.51%–1.00%), low-medium sulfur coal (1.01%–1.50%), medium sulfur coal (1.51%–2.00%), medium-high sulfur coal (2.01%–3.00%), and high sulfur coal (>3.00%). The classical coal facies parameter models proposed by Diessel and Calder were introduced [25,26], and four core indices were selected to quantitatively characterize the peat-forming environments of the Shanxi Formation coal seams. The calculation formulas of each parameter are listed as follows:

Tissue Preservation Index (TPI):

$$\mathrm{TPI} = \frac{\text{telinite} + \text{collinite} + \text{fusinite} + \text{semifusinite}}{\text{desmocollinite} + \text{vitrodetrinite} + \text{corpocollinite} + \text{telocollinite} + \text{inertodetrinite} + \text{macrinite}} \quad (2)$$

Gelification Index (GI):

$$\mathrm{GI} = \frac{\text{total vitrinite} + \text{macrinite}}{\text{fusinite} + \text{semifusinite} + \text{inertodetrinite}} \quad (3)$$

Groundwater Influence Index (GWI):

$$\mathrm{GWI} = \frac{\text{vitrodetrinite} + \text{corpocollinite} + \text{telocollinite} + \text{clay minerals} + \text{quartz}}{\text{telinite} + \text{collinite} + \text{desmocollinite}} \quad (4)$$

Vegetation Index (VI):

$$\mathrm{VI} = \frac{\text{telinite} + \text{collinite} + \text{telocollinite} + \text{fusinite} + \text{semifusinite} + \text{resinite} + \text{suberinite}}{\text{desmocollinite} + \text{vitrodetrinite} + \text{inertodetrinite} + \text{liptodetrinite} + \text{sporinite} + \text{cutinite}} \quad (5)$$

Using auxiliary parameters such as the vitrinite/inertinite ratio (V/I) and the oxidation index (OI), the measured and calculated results for each stratigraphic section are plotted on the GI-TPI and GWI-VI coal facies discrimination diagrams.

Table 2. Proximate, ultimate and sulfur data of No.5 coal.

Sample	FC_{daf}	M_{ad}	A_d	V_{daf}	C_{daf}	H_{daf}	N_{daf}	$S_{t,d}$
D3-4-1	88.37	1.00	4.78	6.85	83.41	3.43	1.39	0.36
D3-4-2	42.12	0.80	47.75	10.13	83.16	3.38	1.48	0.49
D3-4-3	5.79	1.89	83.74	8.59	82.49	3.59	1.39	0.35
D3-4-4	6.01	1.76	83.50	8.74	84.21	3.27	1.31	0.42
D5-1-1	84.68	0.86	8.20	6.40	82.95	2.99	1.31	0.81
D5-1-2	83.93	0.86	8.37	6.98	84.36	3.19	1.20	0.73
D7-11-1	76.94	0.64	15.23	7.34	76.29	3.14	1.17	0.53
D7-11-2	80.59	0.73	11.45	7.37	77.31	3.08	1.06	0.48
D57-1	71.99	0.84	20.28	6.89	78.30	2.88	1.28	0.53
D57-2	85.64	1.20	7.32	5.84	79.48	3.12	1.35	0.57
D57-3	89.19	1.25	3.84	5.72	79.74	3.17	1.47	0.48
D57-4	87.14	1.15	5.65	6.06	82.05	3.07	1.37	0.44
D57-5	80.90	1.42	10.92	6.76	82.12	3.19	1.31	0.51
D57-6	82.15	1.20	10.78	5.87	81.06	3.11	1.37	0.43
D61-1	83.50	1.05	9.09	6.36	83.88	2.98	1.17	0.39
D61-2	84.08	1.07	8.45	6.40	84.06	3.11	1.29	0.56
D61-3	79.61	0.98	12.51	6.90	78.65	3.29	1.48	0.49
D61-4	67.21	0.85	24.43	7.51	81.32	3.31	1.41	0.45
D62-1	86.39	1.96	6.20	7.41	84.86	3.23	1.32	0.38
D62-2	82.52	1.88	8.12	7.79	82.13	3.18	1.12	0.42
D63-1	81.16	1.11	11.15	6.79	81.48	3.15	1.23	0.32
D63-2	83.86	1.23	8.40	6.71	83.41	3.14	1.21	0.32
D63-3	59.79	1.01	31.08	8.52	62.35	2.75	1.01	0.25
D63-4	72.28	1.10	19.28	7.63	71.63	2.81	1.32	0.30
D63-5	79.88	1.10	12.77	6.46	80.18	2.91	1.29	0.32
D64-1	87.77	0.33	4.94	7.01	88.50	3.32	1.45	0.20
D64-2	83.00	0.72	9.16	7.24	79.58	3.09	1.09	0.31
D64-3	77.77	0.53	14.08	7.74	82.25	3.31	1.19	0.27

4. Results and Discussion

4.1. Sequence Stratigraphy and Sedimentary Evolution of the Shanxi Formation

4.1.1. Sequence Stratigraphic Division and Well-Correlation Sedimentary Facies Comparison

Frequent transgressive-regressive cycles and highly heterogeneous interbedded sand-mud strata widely develop in the marine–continental transitional meandering river delta front–lagoon depositional system [27–29]. Well D26 is selected as the standard reference section for high-frequency sequence classification. Combined with the high-resolution identification advantage of INPEFA and the multi-scale time–frequency response of WT in depth and frequency domains, as well as GR spectral evolution features, this study systematically extracts inflection points of sedimentary base-level cycles. Four fourth-order sequences constrained by key sequence boundaries are quantitatively identified within S2, named $S2^4$, $S2^3$, $S2^2$ and $S2^1$ from bottom to top (Figure 2).

$S2^4$ is the lowermost sublayer of S2 and directly overlies the Taiyuan Formation. This interval corresponds to the lowstand systems tract (LST) formed after the termination of marine deposition in the Taiyuan Formation. INPEFA curves exhibit a persistent negative trend, which indicates that the accommodation growth rate was lower than the accumulation rate of terrigenous clastics and peat. This stage represents the initial phase of large-scale progradation of subaqueous distributary channels toward the lagoon within the meandering river delta front. The $S2^3$ and $S2^2$ submembers were deposited during the transgressive systems tract (TST). Lithologies are dominated by dark mudstone and silty mudstone interbedded with thin fine sandstone, which record low-energy subaqueous settings. During

$S2^2$ deposition, the rising rate of sedimentary base level decreased remarkably and tended to be stable. A limited supply of terrigenous clastics weakened the migration and reworking of high-energy distributary channels. As a result, stable long-term peat mires developed in interdistributary bay microfacies in the central-western part of the Daning–Jixian Block. Sharp anomalous signals are detected in well-log time series of the No. 5 coal interval. The corresponding INPEFA curves show subtle extreme values marking the transition from transgression to weak regression, which indicates a long-term, continuous, semi-enclosed, reducing low-energy peat-forming environment within interdistributary bays in this study area. The $S2^1$ submember was deposited during the falling-stage systems tract (FSST), when relative sea level declined and terrigenous sediment supply from the source area was restored. Wavelet coefficients of this interval show regular alternating patterns, while INPEFA curves maintain a persistent negative trend. These geophysical signals record intense progradation and frequent lateral migration of subaqueous distributary channels, which destroyed the early stable peat mires within interdistributary bays. Instead, high-energy delta-front microfacies dominated, including subaqueous distributary channels and overbank sandstones.

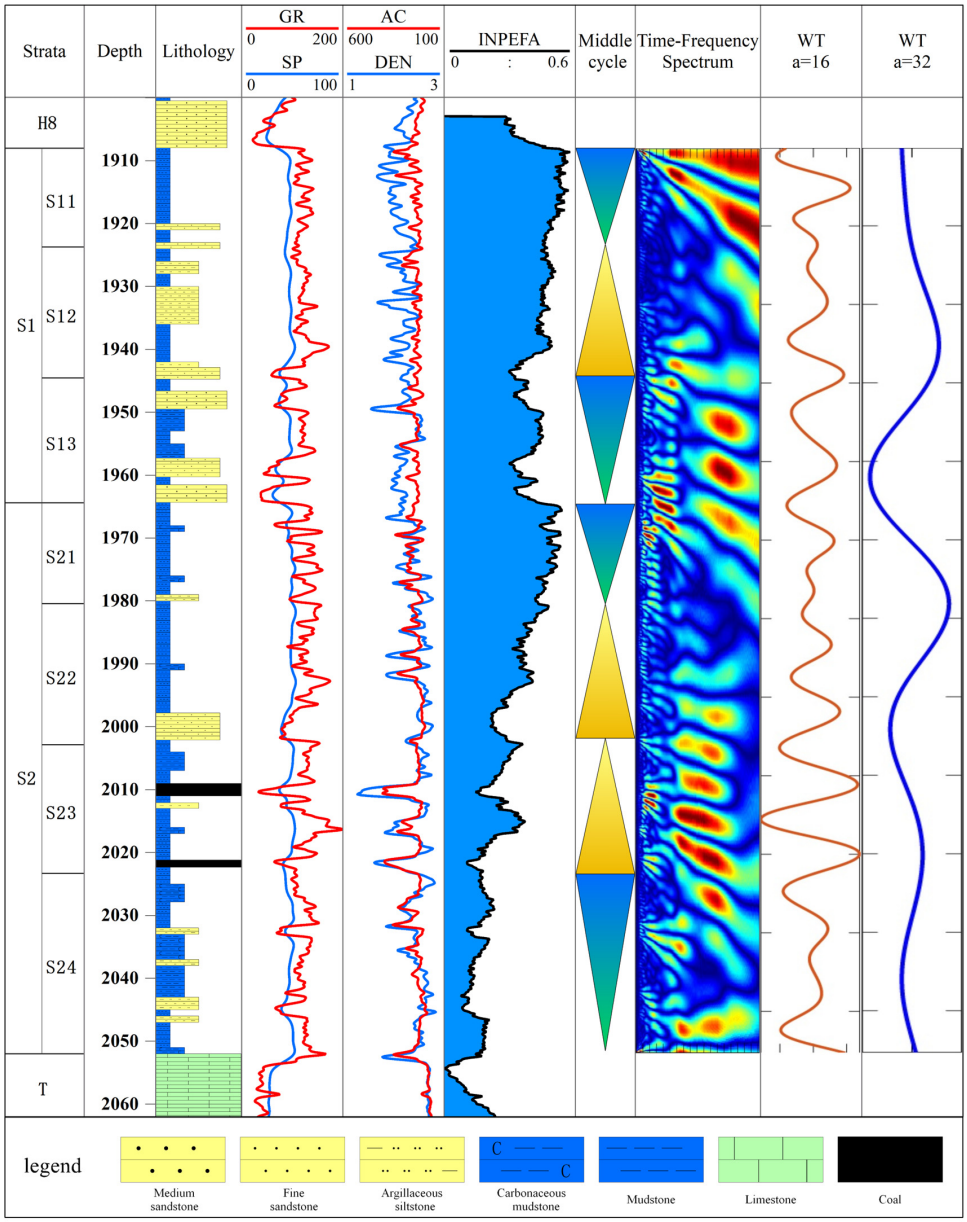


Figure 2. Comprehensive stratigraphic column of the Shanxi Formation in the Daning–Jixian Block.

Previous studies have verified that the Shanxi Formation of the Ordos Basin developed within a marine–continental transitional depositional system under the background of continuous regression of an epicontinental sea [30,31]. Laterally, multiple sedimentary assemblages including braided deltas, meandering river deltas, and barrier coasts were widely distributed. Conventional meandering river delta fronts feature relatively deep water bodies with frequent hydrodynamic disturbances from tides and fluvial currents, and only thin discontinuous coal seams can form in interdistributary bays in most areas [32,33]. Nevertheless, the paleotopography was gentle and sea-level fluctuation amplitudes were limited during the deposition of S2 in the Daning–Jixian Block, giving rise to a typical meandering river delta front–lagoon depositional system. Among these facies, lagoons formed low-energy, sheltered water bodies landward of coastal barriers. In contrast, depressions of interdistributary bays maintained long-term stable and desalinated water conditions, which sustained continuous peat accumulation and enabled the formation of persistent coal beds. Such interdistributary bays constitute the primary peat-forming environments in the study area. Based on core observations, well-log data, and the INPEFA high-frequency isochronous sequence framework established in this work, five microfacies types are finely classified for S2: subaqueous distributary channels, overbank sandstones, mouth bars, interdistributary bays and shallow lagoons. Subaqueous distributary channels act as the framework reservoir sand bodies, while overbank sandstones correspond to thin silty overbank deposits. As low-lying interdistributary-bay depressions became progressively shallower, peat-forming mires developed and became the dominant peat-forming facies.

A north–south well correlation profile parallel to provenance in the central-western Daning–Jixian Block was constructed (Figure 3), which reveals the lateral successive spatial evolution of microfacies along the profile. Subaqueous distributary channel deposits of S2 in the study area exhibit good lateral continuity and relatively large thickness, locally separated by overbank sandstones and argillaceous interdistributary bay deposits. Overbank sand bodies are thin and widely distributed, acting as interlayers that split the channel sand bodies. Two large-scale subaqueous distributary channel sets developed within $S2^4$, which are distributed in the well groups D1–D4-6 and D20–D29, respectively. Thin overbank sandstones occur between the channels, and interdistributary bay mudstones fill the remaining intervals. During $S2^3$ deposition, the base level rose rapidly and water depth increased across the entire study area. Delta lobes retreated northward, with no subaqueous distributary channel sand bodies preserved in the northern strata; overbank sandstones were only concentrated in the well section D6-5–D29. Continuous interdistributary bay mires developed in the northern well section D601–D4-6. The southern interval D10-3–D29 features interbedded overbank sandstones and interdistributary bay deposits, and one set of distributary channels formed under the control of southern provenance. The interdistributary bay depressions in both well intervals possessed moderate water depth and relatively weak tidal disturbance, facilitating coal seam formation. $S2^2$ is dominated by persistent, stable interbeds of interdistributary bay mires and overbank sandstones, which enabled continuous accumulation of the No. 5 main coal seam. Sand bodies and microfacies show limited lateral compartmentalization, forming laterally extensive and stable coal deposits. Two major subaqueous distributary channel sand bodies developed in $S2^1$, occurring in wells D1 and D10–3. Delta-front sand bodies prograded southward again, accompanied by increased sand thickness and thinner overbank sandstone deposits. The distribution of dark mudstones in interdistributary bays shrank, and continuous peat accumulation ceased, terminating the development of the thick No. 5 coal seam; only local carbonaceous mudstones can be observed.

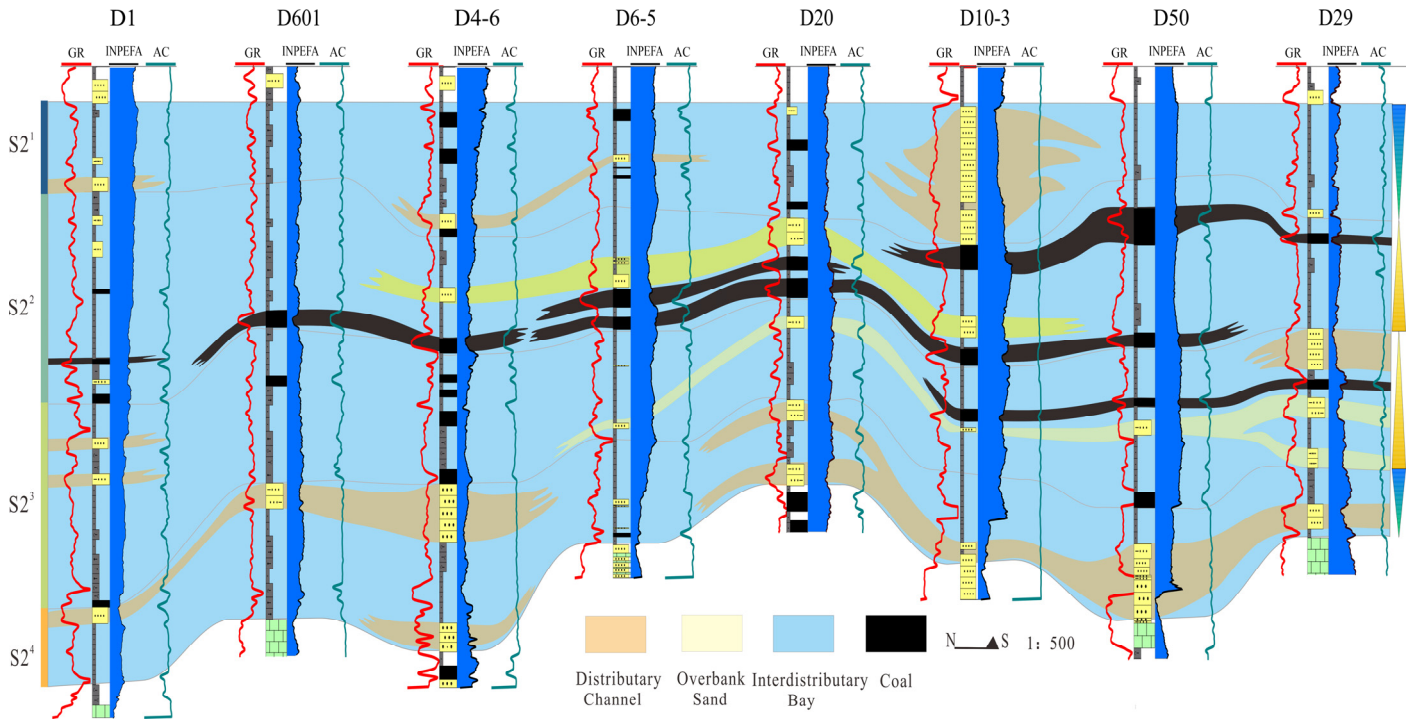


Figure 3. North–south well correlation profile of sedimentary faciesfor the S2, Daning–Jixian Block.

The S2 succession records an evolutionary trend of hydrodynamic conditions: strong → weak → strong. From $S2^4$ to $S2^1$, frequent lateral migration and progradation of subaqueous distributary channels governed the distribution range of interdistributary-bay mires and the spatial geometry of the No. 5 main coal seam.

4.1.2. Paleogeomorphic Characteristics

Paleotopography acts as the dominant factor controlling the spatial distribution of depositional systems, drainage flow directions and accommodation partitioning within coal-bearing basins [6,14,27,28]. Based on high-resolution correlation of well logs, combined with seismic attributes and drilling datasets, the paleotopographic framework of the S2 during its depositional period in the Daning–Jixian Block was reconstructed. The paleotopographic map (Figure 4) reveals that the S2 of the study area presents a microtopographic pattern of "high in the north and east, low in the south and west", with obvious topographic relief and internal differentiation. Relative paleohighs (yellow and red zones) are mainly distributed in the well blocks D19–D24 in the northeastern working area and the eastern margin. These microtopographic paleohighs restrict lateral water expansion and force drainage systems to converge toward low-lying depressions. Relative lowlands (blue and green zones) dominate most of the working area. Two prominent large north–south elongated drainage troughs developed especially along the well zone D4-6–D6-5–D7-6.

The paleotopographic framework provides clear constraints on the locations and distribution patterns of subaqueous distributary channels on the meandering river delta front. By comparing paleotopographic features with channel-distribution trajectories (dashed lines in Figure 4), it can be found that after entering the study area, the northern provenance drainage systems were separated and blocked by microtopographic paleohighs. Major channels prograded sinuously southward and southwestward along low-lying topographic corridors (blue-green zones). Subaqueous distributary channels experienced multi-order branching at well blocks D601 and D3-4 and extended along terrain relief. Meanwhile, deep depressions untouched by channel networks or abandoned after lateral channel

migration featured relatively stagnant and enclosed water bodies, serving as natural settings for large-scale water accumulation and widespread peat swamp development in interdistributary bays in the later stage. The refined reconstruction of paleotopographic patterns provides reliable fundamental geometric constraints for further clarifying the planar distribution of sedimentary microfacies and the migration of coal accumulation centers in each high-frequency sublayer.

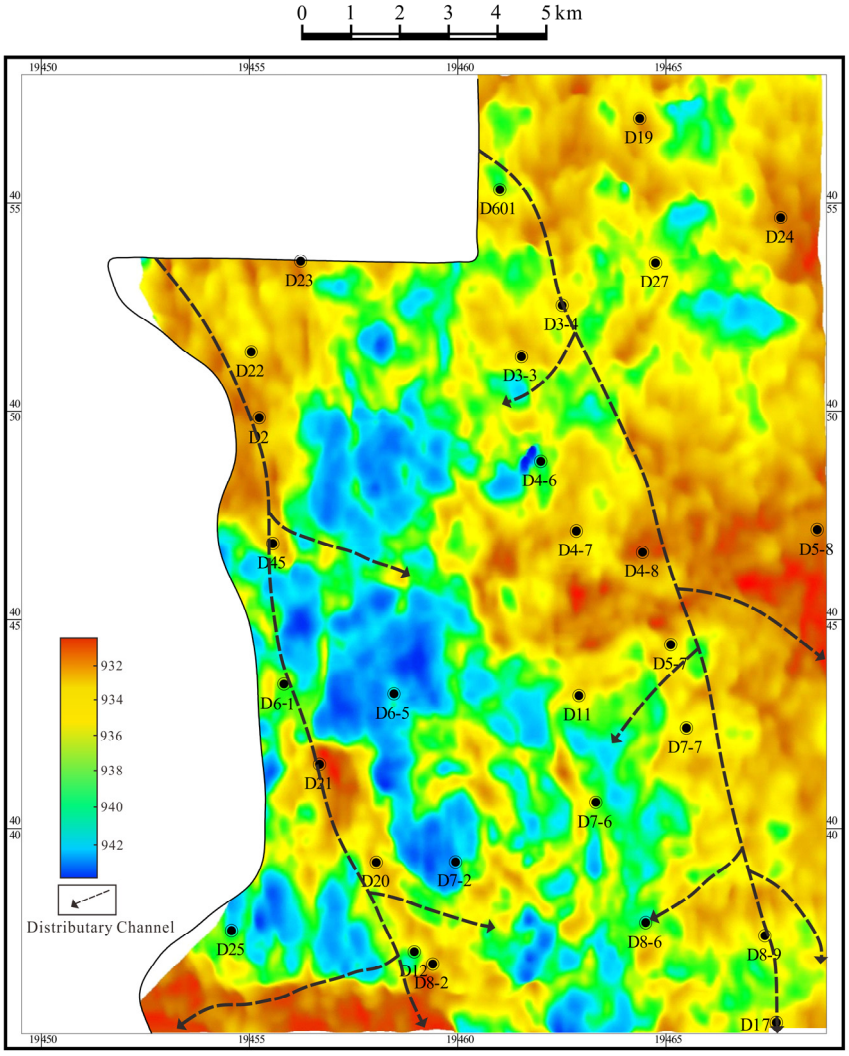


Figure 4. Paleogeomorphology map of the S2, Daning–Jixian Block.

4.1.3. Plan-View Distribution and Evolution of Sedimentary Microfacies

Based on high-frequency cycle identification of single wells and the construction of interwell isochronous frameworks, sand-body distribution ranges are quantitatively characterized by sand-to-stratum ratio contour lines [34,35]. The plan-view distributions of sedimentary microfacies and interdistributary-bay peat-forming microenvironments were mapped for each S2 sublayer ($S2^4$–$S2^1$) (Figure 5). These maps reconstruct the successive evolution of the depositional system. The stage-specific evolution of the plan-view sedimentary architecture indicates that base-level fluctuations, together with variations in sediment supply from the source areas, controlled the spatial differentiation and assemblage of microfacies on the meandering river delta front.

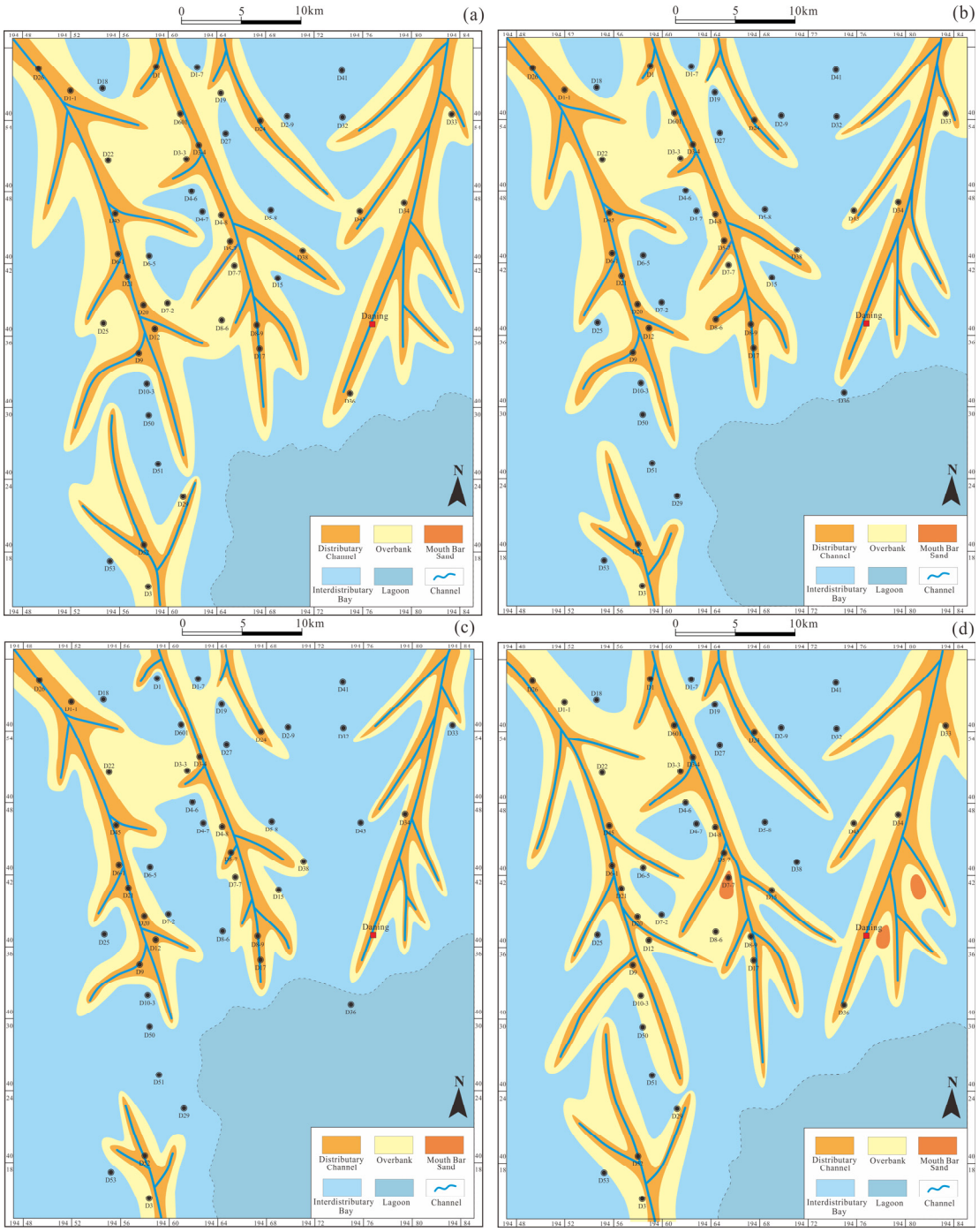


Figure 5. Evolution of plan-view distribution of sedimentary microfacies in the S2 submembers, Daning–Jixian Block: (**a**) $S2^4$; (**b**) $S2^3$; (**c**) $S2^2$; (**d**) $S2^1$.

The $S2^4$ constitutes the first LST at the base of the Shanxi Formation (Figure 5a). During this depositional stage, terrigenous sediment supply from the northern source area was abundant. Subaqueous distributary channels on the meandering river delta front prograded southward toward the lagoon along the main sediment-transport direction. Framework sand bodies formed continuous, broad belts in plan view and were characterized by long transport distances and frequent bifurcation. Overbank sandstones developed along both sides of the major channels. Persistent scouring under strong flow conditions and rapid infilling resulted in well-connected sand bodies, whereas interdistributary-bay microfacies had a very limited plan-view extent. Large, laterally continuous peat-forming

mires had not yet developed within the study block at this stage. The $S2^3$ belongs to the TST (Figure 5b). With continued regional sea-level rise and progressive expansion of accommodation space, basinward progradation of subaqueous distributary channels on the delta front weakened, and the framework sand bodies became markedly less extensive in plan view. Low-energy depressions created by the lateral migration and abandonment of subaqueous distributary channels were rapidly filled with fine-grained argillaceous sediments, forming continuous interdistributary bay deposits covering well blocks D4-6, D4-7 and D7-2. These interdistributary-bay depressions were characterized by lowland topography, restricted water circulation, and low-salinity water. The $S2^2$ corresponds to the evolutionary stage of the TST (Figure 5c). The rate of base-level rise decreased markedly and then remained relatively stable, while terrigenous sediment supply reached a minimum during this depositional cycle. High-energy subaqueous distributary channels migrated laterally and were progressively abandoned, causing a substantial reduction in the plan-view extent of channel sand bodies. Laterally extensive, low-energy interdistributary-bay facies belts developed across well blocks D4-6, D4-7, D6-5, D7-2, and D8-6. These depressions sustained long-term stable sedimentary environments with stagnant water, weakly reducing conditions and low salinity. Such favorable paleogeographic conditions supported prosperous terrestrial peat-forming vegetation and continuous thick peat accumulation. Consequently, the regionally stable No. 5 coal seam developed, with its principal peat-accumulation zones concentrated in interdistributary-bay mires.

The $S2^1$ sublayer records the initial stage of a new high-frequency regressive cycle (Figure 5d). Regional sea level and base level fell continuously, while terrigenous sediment supply from the northern source area recovered and intensified. Subaqueous distributary channels on the meandering river delta front prograded extensively southward, and the framework channel sand bodies displayed an interlaced branching pattern in plan view. Hydrodynamic energy decreased sharply toward the channel front near Well D7-7. Clastic sediments rapidly accumulated to form isolated mouth-bar sand bodies, which constituted delta-front bar deposits in the study block. During southward progradation, high-energy main channels migrated laterally, locally eroded their beds and banks, and reworked associated overbank sandstones. This erosion disrupted the widespread low-energy interdistributary-bay mire paleotopography formed during $S2^2$ deposition. The combined effects of channel scour and continued burial by terrigenous sediments rapidly terminated extensive peat-mire development across the study area. The plan-view sedimentary pattern changed into a heterogeneous composite depositional system comprising subaqueous distributary-channel sand bodies, thin overbank sandstones, isolated mouth bars, and interdistributary-bay mudstones. The facies distributions across all S2 sublayers record the successive evolution of the meandering river delta front: channel progradation and erosion → channel abandonment and bay formation → peat accumulation → secondary progradation. This plan-view evolution demonstrates that the lateral migration and abandonment of subaqueous distributary channels promoted widespread peat-mire development in interdistributary bays and controlled the areal extent and thickness distribution of the No. 5 coal seam.

4.2. Coal Facies Analysis

4.2.1. Maceral Compositions and Microscopic Pore Structure Characteristics

Macrolithological characteristics of coal provide a direct record of peat-mire depositional environments and link macroscopic observations with microscopic maceral features. Core observations of No. 5 coal samples from wells D64, D7-11 and D5-1 in the Daning–Jixian Block (Figure 6) reveal that the coal in the study area is predominantly primary intact coal. The coal cores mostly appear as complete short columns with local broken fragments

in the lower intervals. The coal exhibits a grayish-black to black color with dark brown streaks and generally strong luster. In terms of macroscopic lithotypes, clarain dominates overwhelmingly, followed by durain and vitrain. The coal matrix is moderately hard, locally brittle and fragile, and mostly displays uneven-to-conchoidal fractures. Furthermore, horizontal bedding is widely developed within the coal, accompanied by abundant primary fractures partially filled with calcite and other minerals. Such primary structural signatures dominated by clarain and pervasive horizontal bedding macroscopically indicate that the peat-forming mire was a low-energy, stagnant-water system with weak hydrodynamic conditions and persistent water coverage during peat accumulation. Microscopic maceral assemblages and pore structures further record the evolution of the depositional setting in detail [36–38].

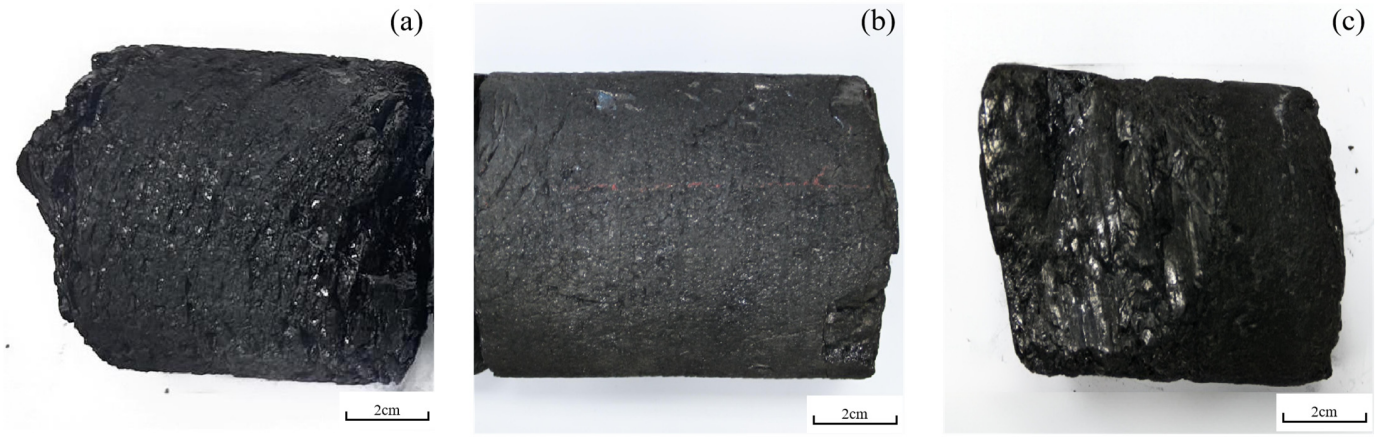


Figure 6. Macro photographs of coal samples from Daning–Jixian Block. (**a**) D64: lithology dominated by clarain with subordinate durain, characterized by uneven fracture, horizontal bedding and locally mineral-filled fractures; (**b**) D5-1: dominated by clarain with subordinate durain, with conchoidal fracture, distinct horizontal bedding and mineral-filled fractures; (**c**) D7-11: dominated by clarain with subordinate vitrain, enriched in vitrinite showing strong greasy luster and well-developed bedding.

Quantitative analysis of coal-petrographic sections shows that the No. 5 coal seam in the S2 of the Daning–Jixian Block is dominated by vitrinite (V), followed by inertinite (I). Liptinite (L) occurs in very low concentrations and is undetectable in most samples. The relative volume fraction of vitrinite ranges from 55% to 95%, whereas that of inertinite is generally between 5% and 35%. All samples contain a certain proportion of inorganic minerals (M), while trace amounts of liptinite occur only at isolated measurement points (Figure 7a). Vitrinite is mainly composed of collinite, desmocollinite, and telinite, whereas inertinite primarily consists of fusinite and semifusinite. The overall enrichment of vitrinite and the widespread occurrence of unstructured vitrinite macerals indicate that the peat-forming mire remained waterlogged, stagnant, and reducing for a prolonged period, promoting intensive gelification of plant remains. In contrast, the persistent occurrence of inertinite suggests that short-term groundwater-level decline or seasonal subaerial exposure and oxidation occurred locally at the interface between interdistributary-bay and lagoonal mires, resulting in the fusinization of some plant tissues [3,36–39].

Observations under an optical microscope and FE-SEM (Figure 8) show that the No. 5 coal seam has a compact matrix containing residual plant-tissue pores, organic pores, and diagenetic microfractures. Collodetrinite commonly forms the matrix surrounding semifusinite fragments, inertodetrinite, and clay minerals. Pore- and fracture-filling minerals are dominated by kaolinite-group clay minerals, whereas carbonate minerals are poorly developed, with only trace calcite observed in samples from Well D64. No framboidal or finely disseminated pyrite characteristic of syngenetic to early-diagenetic

precipitation was identified in the examined samples. Rounded or abraded pyrite grains associated with clastic particles were likewise absent, providing no petrographic evidence for appreciable detrital pyrite input. Coarse crystalline, vein- or fracture-filling pyrite and associated hydrothermal alteration-mineral assemblages were also not observed. The mapped faults are concentrated mainly in the eastern part of the block, away from the principal coal-sampling area (Figure 1c), and the available seismic interpretation shows no fault-related displacement of the No. 5 coal seam within the sampled area. The absence of diagnostic hydrothermal pyrite textures, hydrothermal alteration-mineral assemblages, and fault-related displacement of the target coal seam indicates that fault-controlled hydrothermal activity did not significantly modify the sulfur and pyrite characteristics of the No. 5 coal seam within the study area. Taken together with the low total sulfur contents, clay-dominated mineral assemblage, sedimentary-microfacies distribution, and maceral composition, the scarcity of pyrite supports peat accumulation in a freshwater-dominated, low-energy, weakly reducing environment with limited marine sulfate influence.

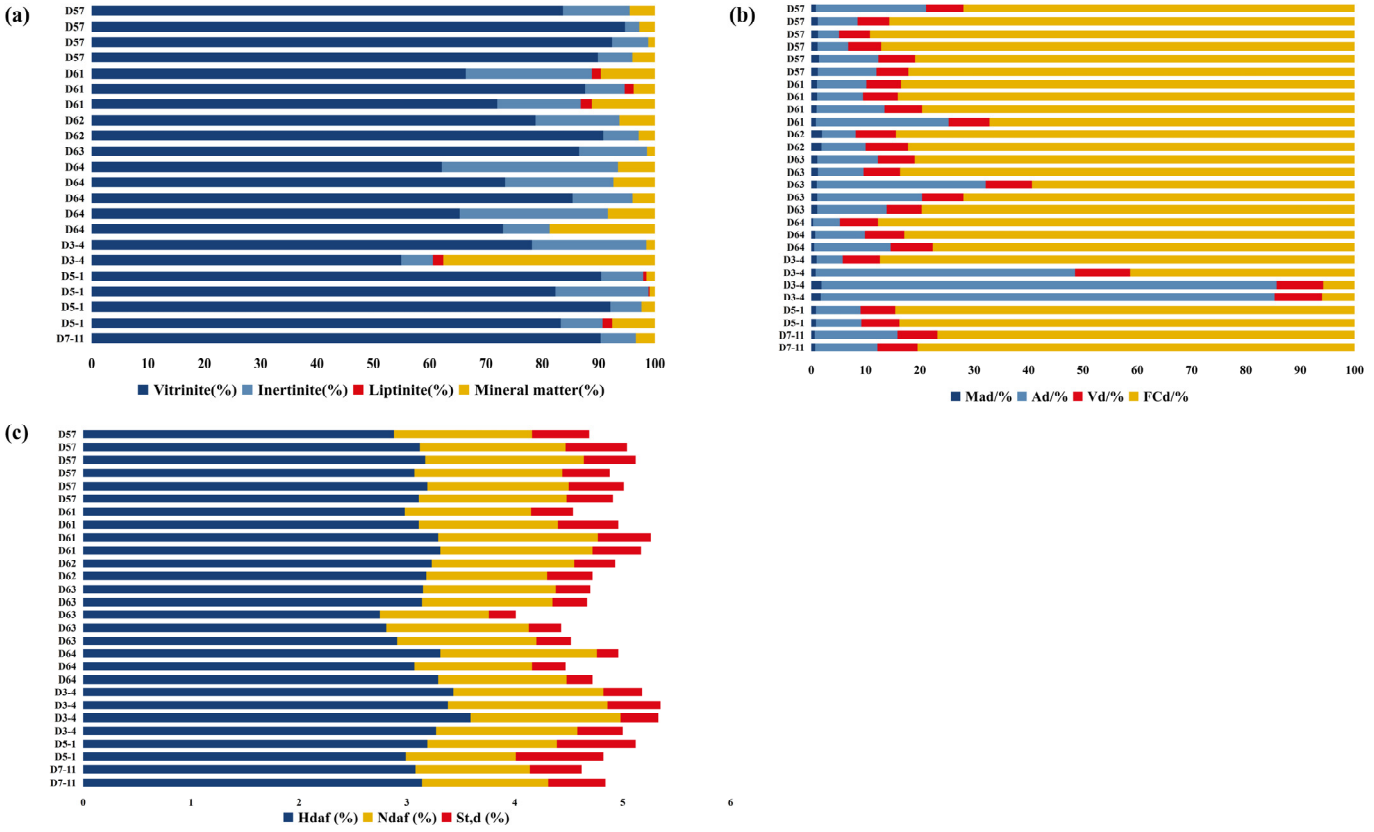


Figure 7. Stacked histograms of coal quality and maceral parameters for No.5 coal seam, Shan 2 Member, Daning–Jixian Block (**a**) Volumetric fractions of organic macerals; (**b**) Proximate analysis indices; (**c**) daf-based elemental contents and total sulfur on dry basis.

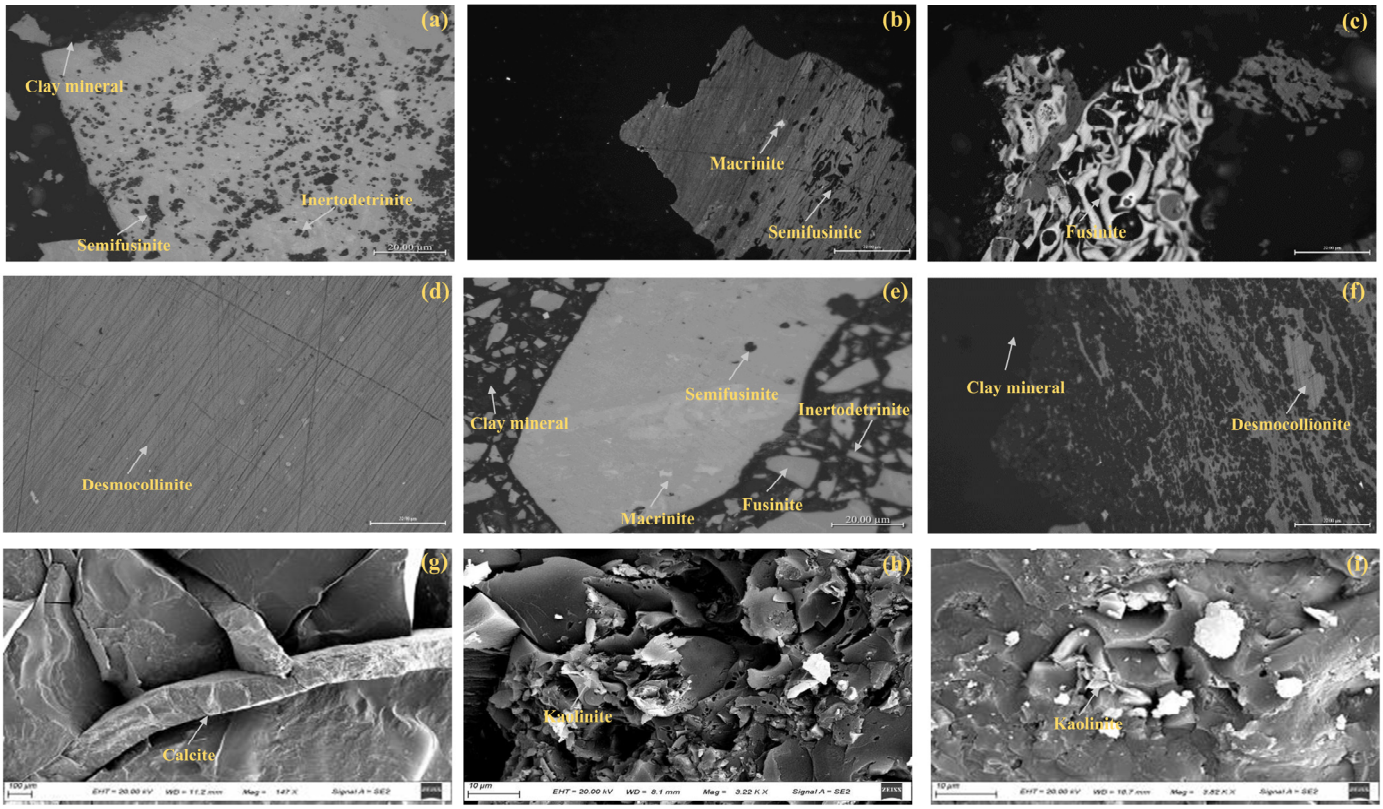


Figure 8. Optical photomicrographs and FE-SEM images of the No. 5 coal seam in the Daning–Jixian Block: (**a**) clay minerals associated with inertodetrinite and semifusinite, Well D61; (**b**) macrinite and semifusinite, Well D63; (**c**) fusinite, Well D62; (**d**) collodetrinite, Well D7-11; (**e**) clay minerals associated with semifusinite, inertodetrinite, macrinite, and fusinite, Well D57; (**f**) clay minerals associated with collodetrinite, Well D3-4; (**g**) calcite, Well D54; (**h**) kaolinite, Well D64; and (**i**) kaolinite, Well D5-1.

4.2.2. Proximate Analysis and Geochemical Characteristics

Proximate analysis and total sulfur data provide constraints on terrigenous sediment input, paleowater salinity, and redox conditions during peat-mire development [21,22]. Stacked histograms of coal-quality data from multiple boreholes show that the No. 5 coal seam in the S2 of the Daning–Jixian Block is characterized by low inherent moisture, moderate-to-low ash yield, and high fixed-carbon content.

The M_{ad} content is generally low and is below 2% in most samples. FC_{daf} is the dominant component, ranging from 60% to 90%, whereas V_{daf} is relatively low and mainly ranges from 5% to 15%. A_d generally ranges from 5% to 20%, indicating low- to medium-low-ash coal. Well D3-4 is the only location where ash yield increases sharply, reaching 83.74% (Figure 7b). Combined with the sedimentary-microfacies distribution shown in Figure 5, this anomalous value is attributed mainly to the location of Well D3-4 within a frequently migrating subaqueous-distributary-channel belt. Large amounts of terrigenous sediment transported by the channels entered adjacent mires during repeated overbank flooding. Inorganic clay minerals were consequently incorporated into the peat deposits, producing locally high-ash coal or transitional carbonaceous-mudstone intervals. After these marginal anomalous data are excluded, the overall low-ash character of the coal seams indicates that weak hydrodynamic conditions prevailed on the meandering river delta front during the main peat-forming stage of $S2^2$. Sheltered by paleotopographic highs, interdistributary-bay mires experienced limited periodic scouring and limited terrigenous sediment input, creating stable conditions for continuous peat accumulation. H_{daf} mainly ranges from 2.8% to 3.5%, whereas N_{daf} varies between 1.0% and 1.5%. The $S_{t,d}$ data indicate

that the No. 5 coal seam generally contains low total sulfur concentrations of 0.2%–1.2%, corresponding to extra-low- to low-sulfur coal (Figure 7c). The low total sulfur content is consistent with limited sulfate availability and freshwater-dominated conditions in the interdistributary-bay mires, although sulfur values may also have been affected by detrital pyrite input and post-depositional alteration. Limited marine sulfate supply may have reduced sulfate-reducing bacterial activity and the formation potential of syngenetic pyrite. This geochemical response is consistent with a low-energy, weakly reducing, freshwater-dominated peat-forming environment within the lagoon–interdistributary-bay system sheltered by paleotopographic highs.

4.2.3. Quantitative Characteristics of Coal-Facies Parameters and Peat-Forming Environment Reconstruction

Quantitative calculation of coal facies indices (TPI, GI, GWI, VI) and cross-plot analysis can accurately reveal the spatial differentiation of microenvironments within peat mires, enabling the reconstruction of peat-forming depositional settings [3,25,26,29]. The coal facies indices derived from quantitative statistics of macerals in No.5 Coal Seam of S2 within the study area display obvious regular environmental differentiation, which effectively characterizes the differences in paleohydrodynamic conditions, vegetation types, and organic matter degradation degree during peat formation. The GI–TPI cross-plot, which constrains waterlogged conditions and the degradation intensity of plant tissues, shows that the coal samples generally have high GI values and a wide range of TPI values. The GI values mainly range from 2.0 to 100 (Figure 9a). These high values indicate that the interdistributary-bay mires maintained a persistently high water table and stagnant, weakly reducing conditions, which promoted intensive gelification of plant remains. This interpretation is consistent with the widespread occurrence of humotelinite and vitrodetrinite in the coal seam. TPI values range from 0.2 to 5.0, reflecting heterogeneity in peat-forming depositional settings. Samples from Wells D61, D63, and some intervals of Well D57 have TPI values below 1.0 and correspond to lowland mire facies. These settings represent persistently waterlogged depressions within interdistributary bays, where thick water coverage and intense microbial degradation limited the preservation of primary plant textures. In contrast, samples from Wells D5-1, D62, D64, and D7-11 have TPI values above 1.0 and correspond to wet forest mires. These areas were characterized by moderate water depth, abundant woody vegetation, and relatively well-preserved plant tissues.

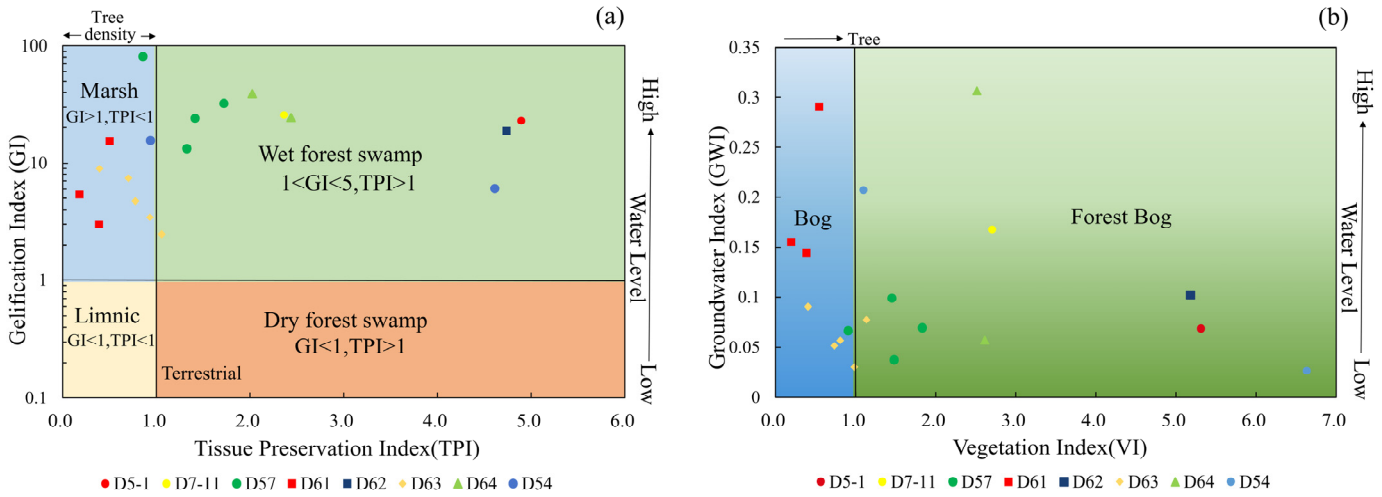


Figure 9. (**a**) GI-TPI Crossplot of GI and TPI for identifying the depositional environment of the coal seam modified [25]. (**b**) Crossplot of VI and GWI for identifying the peat-forming environment modified [25].

The GWI–VI cross-plot further supports the differentiation of these paleoenvironments. The coal samples generally have low GWI values of 0.02–0.15, with a maximum value below 0.35 (Figure 9b). These values indicate weak overbank scouring, limited terrigenous sediment input, and limited groundwater influence within the interdistributary-bay mires. Areas located far from lagoons and adjacent to paleotopographic highs locally developed into oligotrophic mires. This low-energy setting is consistent with the low-ash and low-sulfur geochemical characteristics, indicating that the peat-forming mires were sheltered by paleotopography and were protected from substantial terrigenous sediment input and marine sulfate influence. Most VI values exceed 1.0 and locally exceed 5.0, indicating the stable development of woody vegetation in wet forest mires on microtopographic highs along the margins of interdistributary bays. The GI–TPI cross-plot mainly constrains water depth and redox conditions, whereas the GWI–VI cross-plot characterizes paleohydrodynamics, terrigenous sediment supply, and vegetation differences [25,26,39,40]. Together, these two indices indicate that the No. 5 coal seam in the S2 of the Daning–Jixian Block did not form in a single homogeneous peat-forming environment. Instead, it developed within a composite depositional system in which wet forest mires and herbaceous mires in persistently waterlogged depressions coexisted within a meandering river delta-front–shallow-lagoon framework. During deposition of $S2^2$, base level rose slowly and then remained relatively stable, while subaqueous distributary channels retreated significantly. Microtopographic highs acted as local topographic barriers, promoting the shallowing and stable development of lagoons and interdistributary-bay mires. Herbaceous mires occupied stagnant, persistently waterlogged depressions, whereas wet forest mires developed on microtopographic highs along geomorphic margins. These weakly reducing, freshwater-dominated microenvironments, characterized by long-lived stagnant water and paleotopographic sheltering, restricted intermittent terrigenous sediment input, favored the sustained growth of diverse plant communities, and promoted continued gelification of organic matter. These conditions ultimately favored the development of high-quality, extra-low-ash and extra-low-sulfur coal zones characterized by high GI and extremely low GWI values.

4.3. Relationship Between Depositional Environments and Coal Facies

The regional paleogeographic framework was jointly controlled by sediment supplied from the northern Yinshan Orogenic Belt and the southern Qinling Paleo-uplift (Figure 10a) [14,15]. Alluvial plains and meandering river–delta plains were widely distributed along the northern and southern margins of the basin [41–44]. The Daning–Jixian Block was located in the transition zone between the delta front and shallow lagoon, near the confluence of two fluvial systems with different sediment provenances. This paleogeographic configuration of dual-source convergence and a central lagoonal depression produced a gently sloping depositional surface with widespread low-energy water bodies across the study area. Local paleogeomorphic highs and coastal barriers restricted direct wave and marine influence on the lagoon and interdistributary-bay depressions. These sheltered, low-energy, low-salinity settings provided favorable conditions for the development and preservation of peat-forming mires.

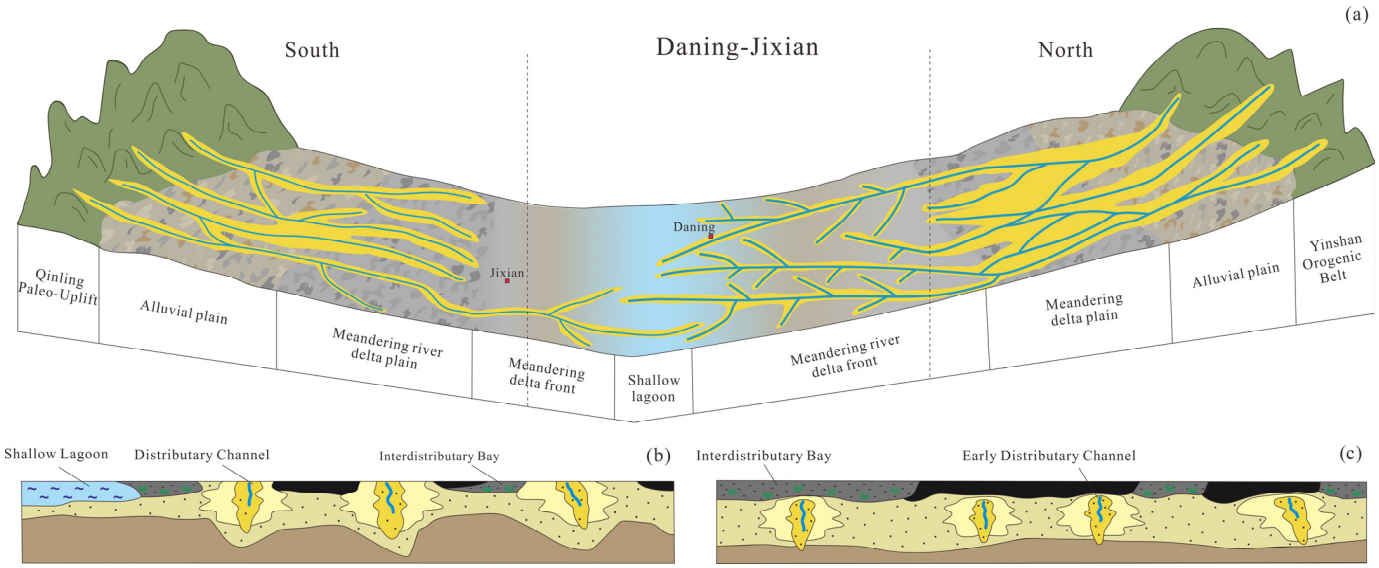


Figure 10. Palaeogeographic framework and coal-accumulation evolution model of meandering river delta front–shallow lagoon for the Shan 2 Member in Daning–Jixian Block: (**a**) 3D palaeogeographic model of bidirectional-source meandering delta system across the southern Qinling Paleo-Uplift and northern Yinshan Orogenic Belt, Daning–Jixian Block; (**b**) scattered peat accumulation during active distributary channel stage; (**c**) contiguous peat accumulation during abandoned channel stage.

In adjacent eastern Ordos blocks, coal accumulation in the Shanxi Formation has generally been interpreted within fluvial–deltaic systems. The Shanxi Formation in the Baode Block is described as a meandering-river–delta-plain swamp succession, whereas the No. 2 coal seam in the South Yanchuan Block is associated mainly with lower-delta-plain lacustrine swamp and water-covered forest-swamp facies. Studies of the Liulin area further indicate that variations among wet-forest, intergradation-forest, drained-forest, and freshwater peat-swamp facies are related to groundwater conditions and peat-mire hydrology [45–47]. At the regional scale, sequence–paleogeographic analysis of the eastern Ordos Basin emphasizes the roles of base-level fluctuations, accommodation space, sediment supply, and basement subsidence in controlling peat accumulation and seam continuity [43,44]. In the Daning–Jixian Block, the No. 5 coal seam shares this regional fluvial–deltaic framework but records a distinct $S2^2$ response, in which channel abandonment, interdistributary-bay infilling, and paleotopographic sheltering promoted the coexistence of wet-forest and deep-water herbaceous mires.

Sedimentary microfacies evolve orderly in both spatial and temporal scales driven by high-frequency base-level cycles [30–35]. This process alters groundwater activity, water depth and terrigenous clastic input within interdistributary peat-forming mires, thereby causing lateral continuity disparities of coal seams and spatial differentiation of coal facies [3,39,40,47]. During base-level fall and intense delta progradation in $S2^4$ and $S2^1$, subaqueous distributary channels prograded basinward and expanded laterally. The depositional system was characterized by strong channelized flows, active sediment transport, frequent overbank flooding, and crevasse-splay deposition. Peat-forming mires were therefore restricted to sheltered, low-lying interdistributary zones. Frequent overbank and crevasse-splay events introduced clay-rich sediment into the mires. Coal seams deposited during this interval were thin and laterally discontinuous, with relatively high GWI values and locally high ash yields, consistent with the data from marginal transitional wells such as D3-4 (Figure 10b). The main peat-forming interval, $S2^2$, was characterized by a slowed and relatively stable base-level rise, resulting in a fundamental change in depositional dynamics. Formerly high-energy subaqueous distributary channels migrated laterally

and were abandoned, while terrigenous sediment flux declined substantially. Under the protection of regional paleogeomorphic highs and continued freshwater input, isolated interdistributary bays and shallow lagoons were gradually filled with fine-grained sediment and became interconnected. Extensive interdistributary-bay peat-forming mires then developed continuously and onlapped abandoned channel sand bodies (Figure 10c). Stagnant, weakly reducing, low-salinity water prevailed across the block during this stage, resulting in generally low GWI values. The stable high water table promoted complete gelification of plant remains and produced coal with high GI values. Controlled by paleotopographic relief, persistently waterlogged interdistributary depressions supported herbaceous mires, whereas abandoned sand bodies and interdistributary microhighs supported wet forest mires. These two coal-facies types therefore occurred in a systematic spatial association. Large-scale, continuous peat accumulation depended on the combined effects of lateral abandonment of meandering river delta-front subaqueous distributary channels, progressive fine-grained infilling, and the expansion of lagoon–interdistributary-bay depressions. The combination of persistently low flow energy, limited sediment transport, restricted water circulation, and long-lived low-salinity water bodies favored widespread and stable preservation of the No. 5 coal seam. The resulting coal-facies assemblage was characterized by high GI, extremely low GWI, extra-low sulfur, and moderate-to-low ash content. From a reservoir perspective, the wet-forest facies favored the preservation of plant-tissue pores and microfractures and thus relatively good pore–fracture connectivity, whereas the more intensely gelified, vitrinite-rich organic matter of the deep-water herbaceous facies provided favorable adsorption sites and enhanced methane retention. This facies-dependent reservoir differentiation is consistent with previous coal-facies studies [40,46–48] and identifies the laterally continuous $S2^2$ peat-forming belt as a priority geological target for deep coalbed methane exploration.

5. Conclusions

By integrating high-frequency time-series analysis of composite logging data, macro-micro sedimentological observations, and multi-index coal geochemical tests, this paper systematically investigates sedimentary evolution and coal facies characteristics of the S2 containing No. 5 coal seam in the deep strata of Daning–Jixian Block. The main conclusions are summarized as follows:

(1) A high-resolution sequence stratigraphic framework and the evolutionary succession of sedimentary microfacies were established. By combining INPEFA and WT techniques, the Shan 2 Member was subdivided into four fourth-order sequences ($S2^4$, $S2^3$, $S2^2$, and $S2^1$). The study area developed a meandering river delta-front–shallow-lagoon depositional system controlled by paleotopography. This system recorded a dynamic evolutionary cycle consisting of distributary-channel progradation and erosion ($S2^4$), bay formation following delta retreat ($S2^3$), fine-grained clastic input and paludification of interdistributary bays during peat accumulation ($S2^2$), and secondary progradation and infilling ($S2^1$).

(2) Maceral assemblages and geochemical signatures of the No. 5 coal seam were characterized in detail. The No. 5 coal seam is dominated by structureless vitrinite and generally exhibits low moisture, moderate-to-low ash yield, and extra-low-to-low sulfur contents, with locally elevated ash yields along channel margins reflecting episodic clastic input. Clay-dominated pore fillings, scarce pyrite, and the absence of hydrothermal pyrite textures or associated alteration minerals support peat accumulation in a freshwater-dominated, low-energy, weakly reducing environment with limited marine sulfate influence and no significant fault-controlled hydrothermal modification.

(3) The peat-forming setting of the composite mires was quantitatively reconstructed. Quantitative coal-facies parameters show that the No. 5 coal seam is characterized by a high Gelification Index (GI = 2.0–100), an extremely low Groundwater Influence Index (GWI = 0.02–0.15), and a wide range of Tissue Preservation Index values (TPI = 0.2–5.0). These indices indicate that the peat-forming mires experienced limited fluvial-flood scouring and developed under long-term stagnant and weakly reducing conditions. Spatially, herbaceous mires in persistently waterlogged depressions coexisted with wet forest mires on interdistributary microhighs, forming a composite coal-facies assemblage.

(4) A coupled coal-accumulation mechanism involving "topographic sheltering–channel abandonment–interdistributary-bay infilling" was proposed. During $S2^2$, the lateral abandonment of subaqueous distributary channels and progressive infilling of sheltered lagoon–interdistributary-bay depressions promoted the development of a laterally continuous peat-forming belt. The higher-TPI wet-forest facies favored the preservation of plant-tissue pores and microfractures, whereas the more strongly gelified deep-water herbaceous facies favored organic micropore development and methane adsorption and retention. The laterally continuous $S2^2$ peat-forming belt therefore represents a priority geological target for deep coalbed methane exploration.

Author Contributions: Conceptualization, W.H. and S.J.; methodology, W.H. and L.Z.; software, X.S. and S.L.; validation, L.Z., Z.Z. and X.S.; formal analysis, Y.W. and J.Y.; investigation, S.L. and Z.Z.; resources, Y.W.; data curation, M.W. and Y.W.; writing—original draft preparation, W.H. and J.Y.; writing—review and editing, W.H. and J.Y.; visualization, L.Z.; supervision, W.H.; project administration, W.H. and S.J.; funding acquisition, W.H., M.W. and S.J. All authors have read and agreed to the published version of the manuscript.

Funding: This research was funded by the National Science and Technology Major Project (Oil & Gas Major Project), grant number 2025ZD1405700, and the Open Fund of China United Coalbed Methane National Engineering Research Center Co., Ltd., grant number GWDC-WB-2025-ZBZX-FR-00104.

Data Availability Statement: The original contributions presented in this study are included in the article. Further inquiries can be directed to the corresponding author.

Acknowledgments: The authors are grateful to China United Coalbed Methane National Engineering Research Center Co., Ltd. for providing well-logging data and coal samples for this study. We would like to thank the technical staff for their assistance in coal petrography testing and experimental analysis. We also appreciate the valuable suggestions and comments from the anonymous reviewers and editors for improving the quality of this manuscript.

Conflicts of Interest: The authors Wei Hou, Mansheng Wu, Lei Zhang, Yuan Wang, Shan Jiang, Shirui Liu, Zengping Zhao, Jie Yin and Xiaosong Shi received funding/financial support from China United Coalbed Methane National Engineering Research Center Co., Ltd. and PetroChina Coalbed Methane Company Limited. The funding sponsors had no role in the design of the study; in the collection, analyses, or interpretation of data; in the writing of the manuscript, and in the decision to publish the results.

References

1. Xiong, X.Y.; Yan, X.; Xu, F.Y.; Li, S.G.; Nie, Z.H.; Feng, Y.Q.; Liu, Y.; Chen, M.; Sun, J.Y.; Zhou, K.; et al. Analysis of multi-factor coupling control mechanism, desorption law and development effect of deep coalbed methane. *Acta Pet. Sin.* **2023**, *44*, 1812–1826. [CrossRef]
2. Li, S.; Qin, Y.; Tang, D.; Shen, J.; Wang, J.; Chen, S. A comprehensive review of deep coalbed methane and recent developments in China. *Int. J. Coal Geol.* **2023**, *279*, 104369. [CrossRef]
3. Dai, S.; Bechtel, A.; Eble, C.F.; Flores, R.M.; French, D.; Graham, I.T.; Hood, M.M.; Hower, J.C.; Korasidis, V.A.; Moore, T.A.; et al. Recognition of peat depositional environments in coal: A review. *Int. J. Coal Geol.* **2020**, *219*, 103383. [CrossRef]

4. Sun, Q.P.; Wang, S.W. The depositional environment analysis of the coal-bearing strata and its significance to coalbed methane development in the Daning–Jixian region. *Nat. Gas. Geosci.* **2006**, *17*, 874–879. (In Chinese)
5. Sun, Y.; Jiang, Y.Q.; Xiong, X.Y.; Li, X.T.; Li, S.X.; Qiu, Z.; Sun, X.W. Lithofacies and sedimentary-environment evolution of the Shan 2^3 submember transitional shale of the Shanxi Formation in the Daning–Jixian area, eastern Ordos Basin. *Coal Geol. Explor.* **2022**, *50*, 104–114. [CrossRef]
6. Li, J.; Li, X.; Tian, W.; Liu, Y.; Wang, H.; Zhang, Y. Characterization of the sedimentary environment of the Shanxi Formation in the southeastern Ordos Basin revealed by detrital-zircon and geochemical analyses. *Minerals* **2023**, *13*, 1331. [CrossRef]
7. Nio, S.D.; Brouwer, J.; Smith, D.; de Jong, M.; Böhm, A. Spectral trend attribute analysis: Applications in the stratigraphic analysis of wireline logs. *First Break* **2005**, *23*, 71–75. [CrossRef]
8. Yu, Z.; Wang, Z.; Wang, J. Continuous wavelet transform and dynamic time warping-based fine division and correlation of glutenite sedimentary cycles. *Math. Geosci.* **2023**, *55*, 521–539. [CrossRef]
9. Li, W.; Zhang, J.; Xie, J.; Xia, Y.; He, Y. Application of the wavelet transform and INPEFA in sequence stratigraphy. *ACS Omega* **2023**, *8*, 3441–3451. [CrossRef]
10. Wang, R.; Xie, J.; Ran, A.; Wang, M.; Dong, Y.; Wang, Z.; Duan, Y. Comparison of INPEFA technology and wavelet transform in sequence-stratigraphic division of a mixed reservoir. *J. Pet. Explor. Prod. Technol.* **2022**, *12*, 3213–3225. [CrossRef]
11. Abbasi, A.; Kodkhodaie, A.; Mahari, R.; Moussavi-Harami, R. Maximum entropy spectral analysis of gamma-ray logs for cyclostratigraphic analysis of the Sarvak Formation. *Earth Sci. Inform.* **2024**, *17*, 1–20. [CrossRef]
12. Li, L.; Wang, Z.Z.; Yin, S.D.; Liu, Y.; Zhang, L.; Hu, Y. Selection and application of wavelet transform in high-frequency sequence-stratigraphic analysis of coarse-grained sediments. *Pet. Sci.* **2024**, *21*, 3016–3028. [CrossRef]
13. Tang, X.; Zhang, J.; Shan, Y.; Xiong, J. Upper Paleozoic coal measures and unconventional natural-gas systems of the Ordos Basin, China. *Geosci. Front.* **2012**, *3*, 863–873. [CrossRef]
14. Zhai, Y.H.; He, D.F.; Kai, B.Z. Tectono-depositional environment and prototype-basin evolution in the Ordos Basin and adjacent areas during the Early Permian. *Earth Sci. Front.* **2023**, *30*, 139–153. [CrossRef]
15. He, F.Q.; Wang, F.B.; Guo, L.G.; An, C. Evolution of the Paleozoic prototype basin and changes in the tectono-sedimentary framework of the Ordos Basin. *Pet. Geol. Exp.* **2022**, *44*, 373–384. [CrossRef]
16. Nie, Z.H.; Wang, D.Z.; Xiong, X.Y.; Yan, X.; Li, S.G.; Feng, Y.Q.; Liu, Y.; Chen, M.; Zhou, K.; Li, C.H. High-efficiency development strategy and engineering practice of deep coal-rock gas using clustered vertical-deviated wells: A case study of the Yichuan well area in the Daning–Jixian Block. *China Pet. Explor.* **2025**, *30*, 120–140. [CrossRef]
17. Wang, T.; Tian, F.; Deng, Z.; Hu, H. The characteristic development of micropores in deep coal and its relationship with adsorption capacity on the eastern margin of the Ordos Basin, China. *Minerals* **2023**, *13*, 302. [CrossRef]
18. *ISO 7404-3:2009*; Methods for the Petrographic Analysis of Coals—Part 3: Method of Determining Maceral Group Composition. International Organization for Standardization: Geneva, Switzerland, 2009.
19. International Committee for Coal and Organic Petrology. The new vitrinite classification (ICCP System 1994). *Fuel* **1998**, *77*, 349–358. [CrossRef]
20. International Committee for Coal and Organic Petrology. The new inertinite classification (ICCP System 1994). *Fuel* **2001**, *80*, 459–471. [CrossRef]
21. Ward, C.R. Analysis and significance of mineral matter in coal seams. *Int. J. Coal Geol.* **2002**, *50*, 135–168. [CrossRef]
22. Chou, C.L. Sulfur in coals: A review of geochemistry and origins. *Int. J. Coal Geol.* **2012**, *100*, 1–13. [CrossRef]
23. *GB/T 30732-2014*; Proximate Analysis of Coal—Instrumental Method. Standardization Administration of China: Beijing, China, 2014.
24. *GB/T 214-2007*; Determination of Total Sulfur in Coal. Standardization Administration of China: Beijing, China, 2007.
25. Diessel, C.F.K. *Coal-Bearing Depositional Systems*; Springer: Berlin/Heidelberg, Germany, 1992. [CrossRef]
26. Calder, J.H.; Gibling, M.R.; Mukhopadhyay, P.K. Peat formation in a Westphalian B piedmont setting, Cumberland Basin, Nova Scotia: Implications for the maceral-based interpretation of rheotrophic and raised paleomires. *Bull. Soc. Géol. Fr.* **1991**, *162*, 283–298.
27. Wang, X.; Zhou, L.; Wu, Y.; Li, S.; Gu, Y.; Li, X. Factors controlling the spatial distribution of complex lithology in transitional shale strata: Implications from logging and 3D seismic data, Shan-2 Lower Submember, eastern Ordos Basin. *Front. Earth Sci.* **2023**, *10*, 951524. [CrossRef]
28. Liang, Y.; Ge, J.; Zhao, X.; Liu, Y.; Zhang, J.; Wang, Y. High-resolution sequence division and its geological significance for exploration of marine–continental transitional shale in Member 2 of the Shanxi Formation, eastern margin of the Ordos Basin. *Nat. Gas. Geosci.* **2022**, *33*, 408–417.
29. Zhang, L.; Huang, L.; Zhao, L.M.; Shu, Z.; He, S.; Chen, M.; Wu, N.; Yang, R. Sedimentary patterns and exploitation practices of tight-sand gas reservoirs in coal-measure strata: A case study of the Shan 2^3 submember in the Daning–Jixian Block. *Coal Geol. Explor.* **2025**, *53*, 114–129. [CrossRef]
30. Hou, Z.S.; Chen, S.Y.; Liang, Z. Sedimentary features and sequence stratigraphy of the successions around the Carboniferous–Permian boundary in the Ordos Basin: Links to glacial and volcanic impacts. *J. Palaeogeogr.* **2023**, *12*, 358–383. [CrossRef]

31. Lu, J.; Shao, L.; Yang, M.; Wang, H.; Qing, K. Sequence paleogeography and coal accumulation in an epicontinental basin. *Int. J. Min. Sci. Technol.* **2013**, *23*, 943–952. [CrossRef]
32. Fielding, C.R. A coal depositional model for the Durham Coal Measures of NE England. *J. Geol. Soc.* **1984**, *141*, 919–931. [CrossRef]
33. Kosters, E.C.; Suter, J.R. Facies relationships and systems tracts in the late Holocene Mississippi Delta Plain. *J. Sediment. Res.* **1993**, *63*, 727–733. [CrossRef]
34. Feng, Z.Z.; Zheng, X.J.; Bao, Z.D.; Zhu, X.M.; Jin, Z.K.; Ji, H.C.; Guan, S.R.; Wang, Y.; Zhang, X.J.; Li, X.P.; et al. Quantitative lithofacies palaeogeography. *J. Palaeogeogr.* **2014**, *3*, 1–34. [CrossRef]
35. Yu, X.H.; Wang, X.Z.; Wang, N.X.; Li, X.B.; Zhang, Y.F.; Zhang, H. Sequence-stratigraphic framework and sedimentary evolution of gas-bearing sand bodies in the Upper Paleozoic of the southeastern Ordos Basin. *J. Palaeogeogr.* **2017**, *19*, 935–954.
36. Farhaduzzaman, M.; Abdullah, W.H.; Islam, M.A. Petrographic characteristics and palaeoenvironment of the Permian coal resources of the Barapukuria and Dighipara Basins, Bangladesh. *J. Asian Earth Sci.* **2013**, *64*, 272–287. [CrossRef]
37. Silva, M.B.; Kalkreuth, W. Petrological and geochemical characterization of Candiota coal seams, Brazil—Implications for coal-facies interpretations and coal rank. *Int. J. Coal Geol.* **2005**, *64*, 217–238. [CrossRef]
38. Toprak, S.; Sütcü, E.C.; Şengüler, İ. A fault-controlled, newly discovered Eskişehir–Alpu coal basin in Turkey: Petrographical properties and depositional environment. *Int. J. Coal Geol.* **2015**, *138*, 127–144. [CrossRef]
39. Sen, S.; Naskar, S.; Das, S. Discussion on the concepts in paleoenvironmental reconstruction from coal macerals and petrographic indices. *Mar. Pet. Geol.* **2016**, *73*, 371–391. [CrossRef]
40. Zhao, L.; Qin, Y.; Cai, C.; Xie, Y.W.; Wang, G.; Huang, B.; Xu, C.L. Control of coal facies on the adsorption–desorption divergence of coals: A case from the Xiqu drainage area, Gujiao CBM Block, North China. *Int. J. Coal Geol.* **2017**, *171*, 169–184. [CrossRef]
41. Shao, L.Y.; Yang, Z.Y.; Shang, X.X.; Xiao, Z.H.; Lu, J.; He, Z.P.; Wang, H.; Zhang, P.F. Lithofacies palaeogeography of the Carboniferous and Permian in the Qinshui Basin, Shanxi Province, China. *J. Palaeogeogr.* **2015**, *4*, 384–412. [CrossRef]
42. Guo, Y.Q.; Zhao, L.S.; Guo, B.C.; Zhang, X.; Liu, Y.; Li, W. Sedimentary characteristics of the Lower Permian in the Ordos Basin and adjacent areas. *J. Palaeogeogr.* **2021**, *23*, 65–80.
43. Lu, J.; Shao, L.Y.; Sun, B.; Zhang, P.F.; He, Z.P.; Wang, H. Sequence palaeogeography and coal accumulation of Carboniferous–Permian coal measures in the eastern Ordos Basin. *J. China Coal Soc.* **2012**, *37*, 747–754. [CrossRef]
44. Li, M.P.; Shao, L.Y.; Li, Z.X.; Zhang, P.F.; Wang, H.; Xiao, Z.H. Lithofacies palaeogeography during accumulation of the lower Carboniferous–Permian coal group in North China. *J. China Coal Soc.* **2020**, *45*, 2399–2410. [CrossRef]
45. Hou, Z.S.; Chen, S.Y.; Wang, Y.; Zhang, L.; Liu, J. Sequence stratigraphy and sedimentary-facies characteristics of the Upper Paleozoic in the Baode area, eastern margin of the Ordos Basin. *J. Palaeogeogr.* **2018**, *20*, 231–243.
46. Li, T.; Wu, C.F. Coal-facies characteristics and their control on methane content in the South Yanchuan Block, southeastern Ordos Basin, China. *Int. J. Green Energy* **2017**, *14*, 63–74. [CrossRef]
47. Zhang, S.H.; Tang, S.H.; Tang, D.Z.; Pan, Z.J.; Yang, F. The characteristics of coal-reservoir pores and coal facies in the Liulin district, Hedong Coalfield, China. *Int. J. Coal Geol.* **2010**, *81*, 117–127. [CrossRef]
48. Li, B.; Guo, Y.Q.; Hu, X.; Liu, Y.; Zhang, X.; Wang, H. Pore structure and heterogeneity characteristics of deep coal reservoirs: A case study of the Daning–Jixian Block on the southeastern margin of the Ordos Basin. *Minerals* **2025**, *15*, 116. [CrossRef]

Disclaimer/Publisher's Note: The statements, opinions and data contained in all publications are solely those of the individual author(s) and contributor(s) and not of MDPI and/or the editor(s). MDPI and/or the editor(s) disclaim responsibility for any injury to people or property resulting from any ideas, methods, instructions or products referred to in the content.